Simple route to prepare different core–shell structured silica-based microspheres

Xingfen Chen, Jinli Pang, Guowei Zhou

Key Laboratory of Fine Chemicals in Universities of Shandong, School of Chemistry and Pharmaceutical Engineering, Qilu University of Technology, Jinan 250353, People's Republic of China
E-mail: guoweizhou@hotmail.com

Published in Micro & Nano Letters; Received on 24th February 2015; Revised on 12th April 2015; Accepted on 13th April 2015

Different core–shell structured silica–titania (SiO_2–TiO_2) nanocomposites were successfully synthesised in two successive stages. In the first stage, the core was synthesised by preparing poly[oligo(ethylene glycol)monomethyl ether methacrylate] (POEOMA) on the modified surface of silica nanoparticles (SiO_2–POEOMA). In the second stage, the shell was formed by depositing or coating tetrabutyl titanate (TBT) with SiO_2-polymer to obtain cauliflower-like, cauliflower–pomegranate-like and pomegranate-like SiO_2–POEOMA–TiO_2 microspheres; the weight ratio of added SiO_2–POEOMA to TBT (1:0.146, 0.293 and 0.439) was then adjusted. Later, the polymer layer was removed to obtain the cauliflower-like, cauliflower–pomegranate-like and pomegranate-like core–shell structured SiO_2–TiO_2 microspheres (CMs, CPMs and PMs). X-ray diffraction results showed that the TiO_2 shell was a pure anatase phase. SiO_2–TiO_2 microspheres were also characterised by N_2 adsorption–desorption; the results showed that a pore structure was found in the porous shell. Extensive porosity was generated in the shell because POEOMA was used as a template and pore-forming agent; the structure of CMs, CPMs and PMs remained almost unchanged. These results also showed that pore volumes and specific surface areas of the final products derived from N_2 sorption decreased as the content of TBT increased. PMs with the highest content of TiO_2 showed the most efficient photocatalytic activity.

1. Introduction: Compared with traditional composites, novel multifunctional nanomaterials exhibit new, enhanced and excellent properties (e.g. mechanical, chemical, electrical, rheological, magnetic and optical). Given such properties, these nanomaterials may potentially be applied in biomedicine [1], catalysis [2], drug delivery [3, 4], energy storage [5], water treatment adsorbents [6] and sensors [7, 8]. Composite nanomaterials with well-defined structures that combine the characteristics of each component or achieve cooperatively enhanced performance have been extensively investigated [2, 7]. In particular, core–shell structured nanomaterials have been extensively explored, and various morphologies, such as pomegranate [9–11], raspberry [12, 13], yolk shell (or rattle-type) [4, 14–18], cauliflower [19, 20] and sandwich [15, 21]-like forms, have been revealed.

As metal oxide semiconductors, nanophase titanium dioxide (TiO_2) can facilitate the rate of surface reactions because of its excellent physicochemical properties, high photoactivity, low cost, nontoxicity and photo-corrosion stability. Nanophase TiO_2 is one of the most commonly used photocatalysts in various solar-driven clean energy and environmental technologies [5, 22, 23]. However, the stable mesostructure of TiO_2 is more difficult to obtain than that of silica; hence, preservation of the pore arrangement upon surfactant or template removal is a significant challenge when this semiconductor is used. Template synthesis of mesoporous TiO_2 usually creates amorphous walls; heat treatment performed to activate crystallisation of titania often causes the ordered mesostructure to collapse [24, 25]. The activator regenerated by electron transfer for atom transfer radical polymerisation (ARGET ATRP) is one of the most widely used polymerisation techniques to graft polymers onto the modified surface of silica nanoparticles when preparing polymer-modified SiO_2 nanoparticles [25]. Yin and Zhou [26] successfully prepared poly (2-(dimethylamino) ethylmethacrylate (PDMAEMA)-co-3-dimethyl (methacryloyloxyethyl) ammoniumpropanesulfonate)-grafted silica nanoparticles through grafting of PDMAEMA brushes onto an SiO_2 surface via ARGET ATRP. This and the above method required more complex procedures and crucial reaction conditions than radical-free solution polymerisation. In this Letter, the cauliflower-like (CM), cauliflower–pomegranate-like (CPM) and pomegranate-like (PM) core–shell structured SiO_2–TiO_2 microspheres (CMs, CPMs and PMs) were prepared to obtain TiO_2 shells without collapse, and the photocatalytic activities of the prepared materials were also evaluated. The novelties of the method and core–shell structured SiO_2–TiO_2 microspheres compared with those previously reported mainly include the following aspects. First, fabrication of silica–poly[oligo(ethylene glycol) monomethyl ether methacrylate] (SiO_2–POEOMA) hybrid microspheres can be easily obtained by using the hydrophilic monomer oligo(ethylene glycol)methyl ether methacrylate (OEOMA) through a simple radical-free solution polymerisation process on the modified surface of silica nanoparticles. Second, SiO_2–POEOMA is used as a template to synthesise CPM, CPPM and PPM SiO_2–POEOMA–TiO_2 microspheres; here, tetrabutyl titanate (TBT) is hydrolysed in the POEOMA segments. Core–shell structured SiO_2–TiO_2 microspheres are prepared by thermal removal of POEOMA from the prepared SiO_2–POEOMA–TiO_2. POEOMA is used as a pore-forming agent to synthesise SiO_2–TiO_2 microspheres. Finally, the structures of CMs, CPMs and PMs can be modified by the addition of different amounts of TBT. The SiO_2–TiO_2 microspheres obtained in this work show potential applications in photocatalysis.

2. Experimental: All of the chemicals used were of analytical grade and applied to synthesise photocatalysts without further purification.

Different core–shell structures of SiO_2–TiO_2 photocatalysts were prepared through the following steps. Tetraethoxysilane (TEOS) and TBT were used as precursors of SiO_2 and TiO_2, respectively. Silica nanoparticles with an average diameter of 100 nm were prepared according to a previously described method [27]. The amounts of ethanol (EtOH), H_2O, ammonia solution (NH_4OH) and TEOS added were 100, 8, 10 and 5 ml, respectively, corresponding to an EtOH, H_2O, NH_4OH and TEOS molar ratio of 17:4:2.6:0.2. SiO_2 was then modified sequentially by using vinyl-organosilicon coupling agents, particularly 3-(trimethoxysilyl)propyl methacrylate (MPS) and hydrophilic monomer OEOMA. Potassium persulphate (KPS) was used as the initiator, EtOH was used as the solvent and NH_4OH was used as a catalyst of hydrolysis. The SiO_2–POEOMA obtained was

doi: 10.1049/mnl.2015.0035

placed in a flask containing 50 ml of EtOH and 1 ml of NH_4OH. To obtain different core–shell structures, 0.5, 1.0 or 1.5 ml of TBT was added dropwise to 0.01 g of SiO_2–POEOMA to achieve SiO_2–POEOMA:TBT weight ratios of 1:0.146, 1:0.293 and 1:0.439, respectively [15, 28], with vigorous stirring and then refluxed at 40°C for 24 h. Milk-like precipitates corresponding to the three different core–shell structures of silica-based microspheres (CPMs, CPPMs and PPMs) were obtained. The precipitates were washed twice with EtOH and distilled water, dried at 50°C and calcined at 450°C for 6 h to obtain CMs, CPMs and PMs. Later, the obtained samples were characterised.

The photocatalytic activities of as-prepared CMs, CPMs and PMs were evaluated by photodecomposition of methyl orange (MO) under UV light irradiation. Before UV irradiation was performed, 0.04 g of CM, CPM and PM particles were dispersed into a quartz cup containing 100 ml of MO aqueous solution (30 mg l^{-1}) with the aid of an ultrasonicator for 15 min and then stored in the dark with continuous stirring for 1 h to establish adsorption–desorption equilibrium of MO on the surface of CM, CPM and PM particles. During irradiation, the suspension was vigorously stirred using a magnetic stirrer and bubbled with oxygen at a constant flow rate. This experiment was performed at room temperature. Samples were removed at an interval of 30 min and centrifuged at 8000 rpm for 10 min. The supernatant was placed in a quartz cuvette, and its optical absorption was determined at 463 nm, which is the maximum absorption of MO, using a Shimadzu UV-2600 spectrophotometer.

The crystal structure of the sample was characterised using an X-ray diffractometer (XRD, Bruker D8) with CuKα radiation (35 kV, 30 mA and λ=0.15406 nm). Data were collected from 20° to 70°. Morphological characteristics were analysed using a JEM 2100 transmission electron microscope (TEM) at an accelerating voltage of 200 kV and SUPRA™55 field emission scanning electron microscope (FESEM). Thermogravimetric analysis (TGA) was performed using a TGA1500 DSP-SP instrument at a heating rate of 20°C min^{-1} from room temperature to 800°C under nitrogen atmosphere. N_2 adsorption–desorption was performed using a TriStar 3020 apparatus. The specific surface area (S_{BET}) and pore size distribution of the samples were, respectively, determined using the Brunauer–Emmett–Teller (BET) method and Barrett–Joyner–Halenda (BJH) model.

3. Results and discussion

3.1. Preparation of CMs, CPMs and PMs: Amorphous silica was synthesised using a previously described method [27]. MPS, a polymerisable silane coupling agent, was modified on the silica surface to form SiO_2–MPS. Radical-free aqueous polymerised OEOMA was added to the mixture, thereby forming an intermediate product (SiO_2–POEOMA). TBT was hydrolysed with a hydrophilic intermediate product and a POEOMA segment was removed to obtain the final products (CMs, CPMs and PMs; Fig. 1).

3.2. Characterisation of modified silica: Figs. 2*a* and *b* show the TEM images of spherical SiO_2 and POEOMA grafted onto the bare SiO_2 nanoparticles (SiO_2–POEOMA). Monodispersed spherical SiO_2 with an average diameter of approximately 100 nm was obtained. After POEOMA was grafted onto the modified SiO_2 surface (Fig. 2*b*), SiO_2–POEOMA nanostructures with an average thickness of ∼10 nm may be clearly observed. The obtained SiO_2–POEOMA showed severe aggregation because of POEOMA. This result indicates that hydrophilic POEOMA was successfully grafted onto the SiO_2 surface.

Fig. 3 shows the TGA results of pure SiO_2, SiO_2–MPS and SiO_2–POEOMA. When heated from 0 to 100°C, bare SiO_2 exhibited a total weight loss of 8.04%. This weight loss corresponds to the loss of chemisorbed water on the SiO_2 surface. When heated to 800°C, SiO_2–MPS showed major weight loss of ∼12.11%, which

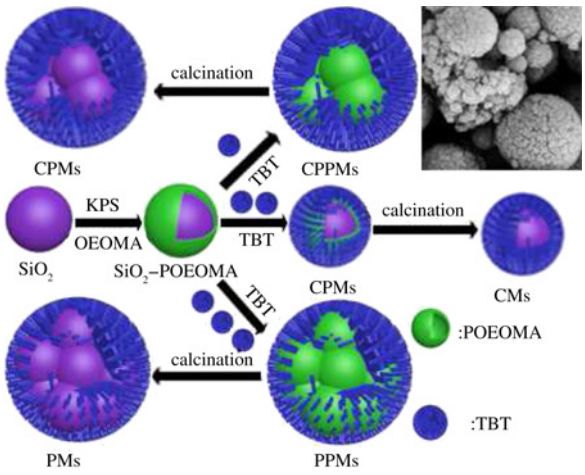

Figure 1 *Schematic of the preparation of CMs, CPMs and PMs*

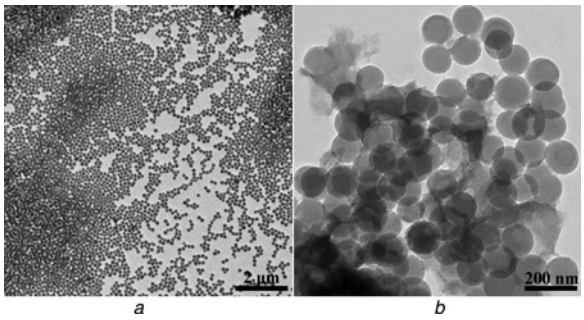

Figure 2 *TEM images*
a SiO_2
b SiO_2–POEOMA

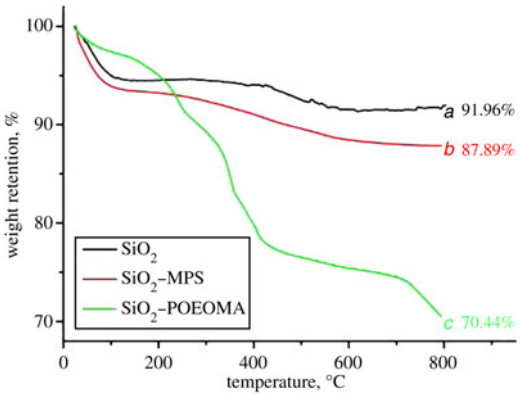

Figure 3 *TGA results*
a SiO_2
b SiO_2–MPS
c SiO_2–POEOMA

indicates that MPS was successfully coated onto the SiO_2 surface (Fig. 3*b*). Fig. 3*c* shows the TG graph of SiO_2–POEOMA. Compared with that of SiO_2–MPS, the weight loss of SiO_2–POEOMA, which is attributed to the dissociation of POEOMA, was about 17.45%. This result indicates that about 17.45 wt% of the available POEOMA was successfully grafted onto the SiO_2 surface.

3.3. Characterisation of CMs, CPMs and PMs: Fig. 4 shows the TEM images of CPMs, CPPMs and PPMs as well as their

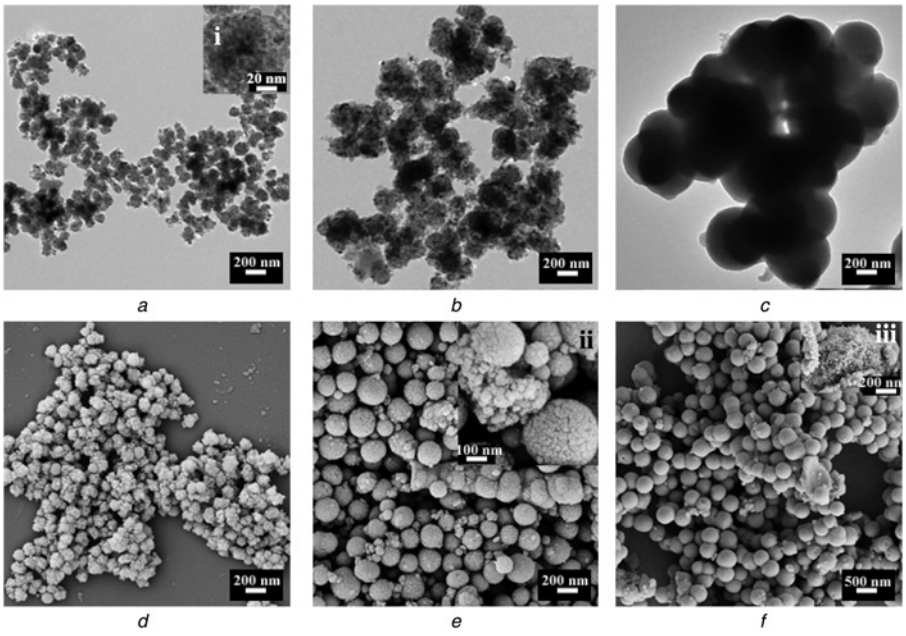

Figure 4 *TEM images and FESEM images of CPMs, CPPMs and PPMs*
a CPMs TEM image
b CPPMs TEM image
c PPMs TEM image
d CMs FESEM image
e CPMs FESEM image
f PMs FESEM image
HRTEM images of inset *i* is at a higher magnification for *a*. The FESEM images of insets *ii* and *iii* are for *e* and *f*

corresponding FESEM images. Figs. 4*a* and *b* show the formation of aggregated secondary CM and CPM particles through agglomeration and precipitation of TiO_2 primary particles on the SiO_2–PEPOMA particle surface. A cauliflower-like structure of CPMs was obtained (Fig. 4*a*, inset *i*). The cauliflower- and pomegranate-like structures of CPPMs were obtained when the weight ratio of TBT:SiO_2–POEOMA was 1:0.293 (Fig. 4*e*, inset *ii*). Another structure of SiO_2–TiO_2, the pomegranate-like structure, formed as the TBT (PMs) added increased further (Fig. 4*f*, inset *iii*). SiO_2–TiO_2 agglomerates exhibited a smooth and porous surface as the content of TBT increased, thereby resulting in a decrease in S_{BET} (Table 1).

The chemical compositions of CMs, CPMs and PMs were determined by XRD to reveal details of their chemical composition and crystallographic structure (Fig. 5). Peaks located at 25.3°, 37.9°, 48.2°, 54.1°, 55.2° and 62.8° were assigned to the 101, 004, 200, 105, 211 and 204 faces of TiO_2 anatase. The XRD results indicate that calcination occurs at 450°C and that the major crystalline phase of the prepared CMs, CPMs and PMs is anatase without any rutile; however, SiO_2 is formed as an amorphous phase [29]. These results further confirm that the addition of SiO_2 to TiO_2 increases the thermal stability of TiO_2 crystallites. However, excess addition of SiO_2 to TiO_2 reduces the crystallinity of TiO_2 anatase; thus, PMs display weak anatase crystallinity.

Table 1 Structural properties of SiO_2–TiO_2 microspheres prepared from SiO_2–POEOMA–TiO_2 microspheres

Sample	S_{BET}, $m^2\ g^{-1}$[a]	V_p, $cm^3\ g^{-1}$[b]	Pore size, nm[b]
CMs	72.28	0.14	7.32
CPMs	38.94	0.06	6.00
PMs	19.63	0.03	6.37

[a]S_{BET} was determined by the multipoint BET method using the adsorption data in the relative pressure (P/P_0) range of 0.05–0.23
[b]Pore volume and average pore size were determined by nitrogen adsorption volume at a relative pressure of 0.99

N_2 adsorption–desorption isotherms and the corresponding BJH pore size distribution curves of CMs, CPMs and PMs are shown in Fig. 6. According to the IUPAC classification, CMs display a type III isotherm and H2 hysteresis, which indicates a mesoporous material that exhibits capillary condensation and evaporation [30]. By contrast, CPMs and PMs showed curves of types I and IV. At relative pressures ranging from 0.4 to 1, the curves revealed two small hysteresis loops. At relatively low pressures of 0.4–0.8, the hysteresis loop was type H2, which suggests the existence of 'ink-bottle' pores [31]; at a relatively high-pressure range of 0.8–1.0, however, the hysteresis loop changes to type H3, which is associated with 'slit-like' pores [32]. Compared with that of PMs, the inflection position of the CPMs shifted slightly towards relatively higher pressures and the volume of adsorbed nitrogen increased; this result suggests a decrease in pore size. The

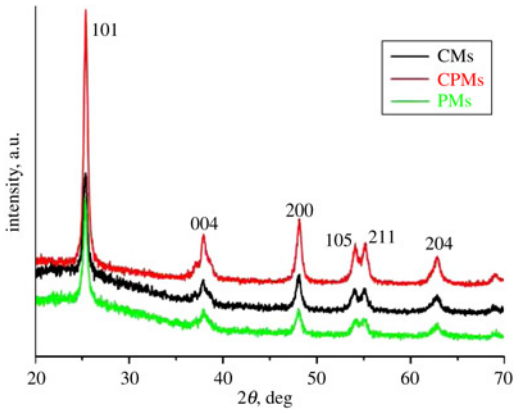

Figure 5 *XRD patterns of CPMs (red line), CMs (black line) and PMs (green line)*

doi: 10.1049/mnl.2015.0035

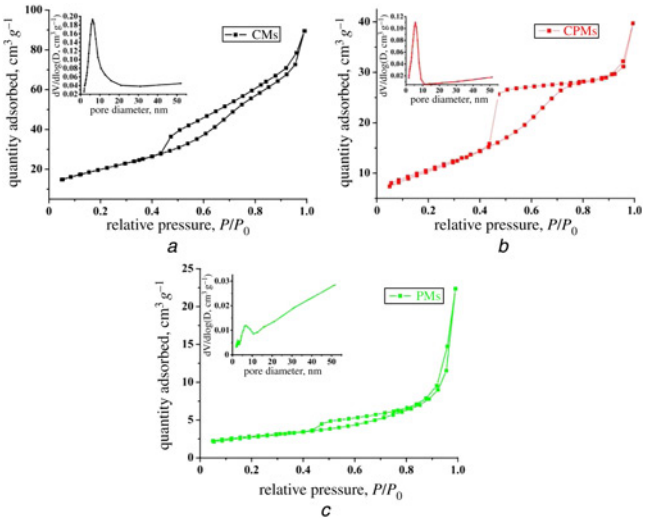

Figure 6 *N_2 adsorption–desorption isotherms and corresponding BJH pore size distribution curves*
a CMs
b CPMs
c PMs

calculated S_{BET}s of CMs, CPMs and PMs were 72.28, 38.94 and 19.63 $m^2 g^{-1}$, respectively (Table 1), and their pore size distributions were 7.32, 6.00 and 6.37 nm, respectively. All of the pores were present in the outer shell of TiO_2 because TBT was hydrolysed with the hydrophilic segment (POEOMA) of SiO_2–POEOMA microspheres. Pores were then generated upon removal of the POEOMA polymer. The quality of absorption decreased as the content of TBT increased.

The photocatalytic activities of CMs, CPMs and PMs are shown in Fig. 7. As the UV irradiation times increased, the concentration of MO in mixtures of CMs, CPMs and PMs and dispersed aqueous MO decreased. The photocatalytic activity of PMs was nearly 100%. This result indicates that higher TiO_2 content results in higher photocatalytic activity. The photocatalytic activity of CMs was higher than that of CPMs. This result also indicates that a larger surface area confers better photocatalytic activity because more active sites are provided for MO molecule adsorption. Thus, the TiO_2 content is superior to the S_{BET} as a factor influencing the photocatalytic activity of the samples.

4. Conclusions: In summary, CMs, CPMs and PMs were successfully prepared. SiO_2–POEOMA was also synthesised for the first time by applying a simple route, namely, radical-free solution polymerisation. This procedure is not only milder but also safer than the approaches described in previous studies. The SiO_2–TiO_2 microspheres obtained showed different photocatalytic activities for MO degradation. In particular, PMs with the highest TiO_2 content showed the most efficient photocatalytic activity. CMs with larger S_{BET} also exhibited higher photocatalytic activities than CPMs.

5. Acknowledgments: This work was supported by the National Natural Science Foundation of China (grant nos. 20976100 and 51372124) and the Program for Scientific Research Innovation Team in Colleges and Universities of Shandong Province.

6 References

[1] Yin P., Zhao M., Deng C.: 'High efficiency enrichment of low–abundance peptides by novel dual-platform graphene@SiO_2@PMMA', *Nanoscale*, 2012, **4**, (22), pp. 6948–6950
[2] Deng Y., Cai Y., Sun Z., *ET AL.*: 'Multifunctional mesoporous composite microspheres with well-designed nanostructure: a highly integrated catalyst system', *J. Am. Chem. Soc.*, 2010, **132**, (24), pp. 8466–8473
[3] Xu Z., Wang D., Guan M., *ET AL.*: 'Photoluminescent silicon nanocrystal-based multifunctional carrier for pH-regulated drug delivery', *ACS Appl. Mater. Inter.*, 2012, **4**, (7), pp. 3424–3431
[4] Zhu Y., Ikoma T., Hanagata N., Kaskel S.: 'Rattle-type Fe_3O_4@SiO_2 hollow mesoporous spheres as carriers for drug delivery', *Small*, 2010, **6**, (3), pp. 471–478
[5] Chen X., Liu L., Peter Y.Y., Mao S.S.: 'Increasing solar absorption for photocatalysis with black hydrogenated titanium dioxide nanocrystals', *Science*, 2011, **331**, (6018), pp. 746–750
[6] Ding J., Li B., Liu Y., *ET AL.*: 'Fabrication of Fe_3O_4@ reduced graphene oxide composite via novel colloid electrostatic self-assembly process for removal of contaminants from water', *J. Mater. Chem. A*, 2015, **3**, (2), pp. 832–839
[7] Wang Y., Li B., Zhang L., Song H.: 'Multifunctional mesoporous nanocomposites with magnetic, optical, and sensing features: synthesis, characterization, and their oxygen-sensing performance', *Langmuir*, 2013, **29**, (4), pp. 1273–1279
[8] He L., Liu Y., Liu J., *ET AL.*: 'Core–shell noble-metal@metal-organic-framework nanoparticles with highly selective sensing property', *Angew. Chem. Int. Edit.*, 2013, **52**, (13), pp. 3741–3745
[9] Luciani C.V., Choi K.Y., Han J.J., Jung Y.: 'Polymer particles with a pomegranate-like internal structure via micro-dispersive polymerization in a geometrically confined reaction space I. experimental study', *Polymer*, 2011, **52**, (4), pp. 942–948
[10] Wang X., Liu D., Song S., Zhang H.: 'Pt@CeO_2 multicore@ shell self-assembled nanospheres: clean synthesis, structure optimization, and catalytic applications', *J. Am. Chem. Soc.*, 2013, **135**, (42), pp. 15864–15872
[11] Luciani C.V., Choi K.Y.: 'Mathematical modeling of polymer particles with a pomegranate-like internal structure via micro-dispersive polymerization in a geometrically confined reaction space', *Macromol. Theor. Simul.*, 2014, **23**, (3), pp. 110–124
[12] Li X., He J.: 'Synthesis of raspberry-like SiO_2–TiO_2 nanoparticles toward antireflective and self-cleaning coatings', *ACS Appl. Mater. Inter.*, 2013, **5**, (11), pp. 5282–5290
[13] Li G., Yang X.: 'Facile synthesis of hollow polymer microspheres with movable cores with the aid of hydrogen-bonding interaction', *J. Phys. Chem. B*, 2007, **111**, (44), pp. 12781–12786
[14] Ren Y., Chen M., Zhang Y., Wu L.: 'Fabrication of rattle-type TiO_2/SiO_2 core/shell particles with both high photoactivity and UV-shielding property', *Langmuir*, 2010, **26**, (13), pp. 11391–11396
[15] Li W., Deng Y., Wu Z., *ET AL.*: 'Hydrothermal etching assisted crystallization: a facile route to functional yolk–shell titanate microspheres with ultrathin nanosheets-assembled double shells', *J. Am. Chem. Soc.*, 2011, **133**, (40), pp. 15830–15833
[16] Yang Y., Liu J., Li X., Liu X., Yang Q.: 'Organosilane-assisted transformation from core–shell to yolk–shell nanocomposites', *Chem. Mater.*, 2011, **23**, (16), pp. 3676–3684
[17] Zhang X., Mansouri S., Clime L., Ly H., Yahia L.H., Veres T.: 'Fe_3O_4–silica core–shell nanoporous particles for high-capacity pH-triggered drug delivery', *J. Mater. Chem.*, 2012, **22**, (29), pp. 14450–14457
[18] Cao L., Chen D., Caruso R.A.: 'Surface-metastable phase-initiated seeding and Ostwald ripening: a facile fluorine-free process towards

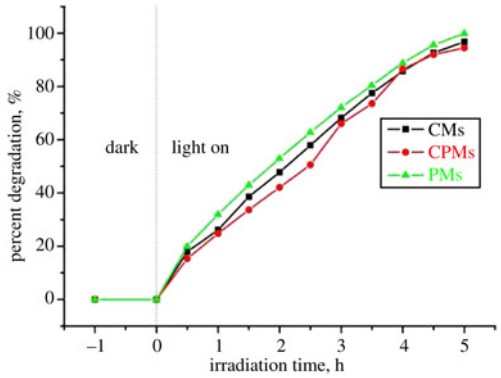

Figure 7 *Per cent degradation of MO as a function of irradiation time for CMs (black square), CPMs (red circle) and PMs (green up-pointing triangle)*

spherical fluffy core/shell, yolk/shell, and hollow anatase nanostructures', *Angew. Chem.*, 2013, **125**, (42), pp. 11192–11197
[19] Jiang Y., Yan Y., Zhang W., Ni L., Sun Y., Yin H.: 'Synthesis of cauliflower-like ZnO–TiO_2 composite porous film and photoelectrical properties', *Appl. Surf. Sci.*, 2011, **257**, (15), pp. 6583–6589
[20] Yang X., Li Q., Zhang S., Zhong X., Dai Y., Luo F.: 'Electrochemical corrosion behaviors and protective properties of Ni–Co–TiO_2 composite coating prepared on sintered NdFeB magnet', *Mater. Corros.*, 2010, **61**, (7), pp. 618–625
[21] Chen J., Wang D., Qi J., *ET AL.*: 'Monodisperse hollow spheres with sandwich heterostructured shells as high-performance catalysts via an extended SiO_2 template method', *Small*, 2015, **11**, (4), pp. 420–425
[22] Chen X., Mao S.S.: 'Titanium dioxide nanomaterials: synthesis, properties, modifications, and applications', *Chem. Rev.*, 2007, **107**, (7), pp. 2891–2959
[23] Chen X., Shen S., Guo L., Mao S.S.: 'Semiconductor-based photocatalytic hydrogen generation', *Chem. Rev.*, 2010, **110**, (11), pp. 6503–6570
[24] Zimny K., Roques-Carmes T., Carteret C., Stébé M., Blin J.: 'Synthesis and photoactivity of ordered mesoporous titania with a semicrystalline framework', *J. Phys. Chem. C*, 2012, **116**, (11), pp. 6585–6594
[25] Zhao M.N., Zhou G.W., Zhang L., Li X.Y., Li T.D., Liu F.F.: 'Fabrication and photoactivity of a tunable-void SiO_2–TiO_2 core–shell structure on modified SiO_2 nanospheres by grafting an amphiphilic diblock copolymer using ARGET ATRP', *Soft. Mater.*, 2014, **10**, (8), pp. 1110–1120
[26] Yin J., Zhou J.C.: 'Novel polyethersulfone hybrid ultrafiltration membrane prepared with SiO_2-g-(PDMAEMA-co-PDMAPS) and its antifouling performances in oil-in-water emulsion application', *Desalination*, 2015, **365**, pp. 46–56
[27] Stöber W., Fink A., Bohn E.: 'Controlled growth of monodisperse silica spheres in the micron size range', *J. Colloid. Interf. Sci.*, 1968, **26**, (1), pp. 62–69
[28] Cheng G., Wang Z.G., Liu Y.L., Zhang J.L., Sun D.H., Ni J.Z.: 'Magnetic affinity microspheres with meso-/macroporous shells for selective enrichment and fast separation of phosphorylated biomolecules', *ACS Appl. Mater. Interfaces*, 2013, **5**, (8), pp. 3182–3190
[29] Sun Z., Bai C., Zheng S., Yang X., Frost R.L.: 'A comparative study of different porous amorphous silica minerals supported TiO_2 catalysts', *Appl. Catal. A, Gen*, 2013, **458**, pp. 103–110
[30] Zhang X., Zhang F., Chan K.Y.: 'Synthesis of titania–silica mixed oxide mesoporous materials, characterization and photocatalytic properties', *Appl. Catal. A, Gen*, 2005, **284**, (1–2), pp. 193–198
[31] Everett D.: 'Manual of symbols and terminology for physicochemical quantities and units, appendix II: definitions, terminology and symbols in colloid and surface chemistry', *Pure Ure. Appl. Chem.*, 1972, **31**, (4), pp. 577–638
[32] Sing K.S.: 'Reporting physisorption data for gas/solid systems with special reference to the determination of surface area and porosity', *Pure Ure. Appl. Chem.*, 1985, **57**, (4), pp. 603–619

doi: 10.1049/mnl.2015.0035